Proc. Natl. Acad. Sci. USA
Vol. 83, pp. 7746–7750, October 1986
Biophysics

Location of the cyclohexene ring of the chromophore of bacteriorhodopsin by neutron diffraction with selectively deuterated retinal

(purple membrane/*Halobacterium halobium*/structure)

F. SEIFF, J. WESTERHAUSEN, I. WALLAT, AND M. P. HEYN

Biophysics Group, Department of Physics, Freie Universität Berlin, Arnimallee 14, D-1000 Berlin 33, Federal Republic of Germany

Communicated by L. N. M. Duysens, June 23, 1986

ABSTRACT **We report on the location of the cyclohexene ring of the retinylidene chromophore of bacteriorhodopsin projected onto the plane of the membrane. For this purpose, partially deuterated retinal was synthesized containing 11 deuterons at the following positions of the cyclohexene ring: one at C-2, two at C-4, three at C-16, three at C-17, and two at C-18. The partially deuterated retinal was incorporated biosynthetically during growth of the bacteria by using the mutant JW5, which is deficient in the synthesis of retinal. Undeuterated samples were prepared in the same way. Characterization by x-ray diffraction and absorption spectroscopy showed that these samples are identical to native purple membranes as judged by these criteria. A Fourier difference map was calculated from the differences in in-plane diffraction intensities between the deuterated and undeuterated dark-adapted membrane samples. Model calculations showed that the observed difference density had the amplitude expected for a label containing 11 deuterons. At 8.7 Å resolution, the map shows one major peak with the center of mass of the deuterated ring in the interior of the molecule between helices 3, 4, 5, and 6. Based on this result and on our previous work on the location of the middle of the polyene chain, we conclude that the COOH-terminal helix G, to which retinal is attached at lysine-216, is either helix 2 or helix 6.**

The chromophore of bacteriorhodopsin is of central importance in the photochemistry and in the charge cycle of this light-driven proton pump (1). Fluorescence energy transfer (2, 3) and neutron diffraction with perdeuterated retinal (4, 5) have been used in attempts to determine the location of retinal in the projected density of bacteriorhodopsin. Since retinal is ≈15 Å long in its all-trans form and since its polyene chain makes an angle of ≈20° with the plane of the membrane (6), the mass density of retinal projected onto the plane of the membrane will be smeared out and elongated. Low-resolution neutron diffraction experiments with perdeuterated retinal (28 deuterons) will therefore determine only the center of deuteration of this delocalized mass distribution. More detailed structural information about the location of the various parts of retinal may be obtained by using partially deuterated retinal. This method was recently applied with a synthetic retinal containing 10 deuterons to determine the position of the middle of the polyene chain (C-11) (7). In the present work, we continue this approach with a synthetic retinal that was selectively labeled with 11 deuterons in the cyclohexene ring to find the location of the ring (Fig. 1). Taken together, the results of these two studies provide a low-resolution map of the arrangement and orientation of the chromophore within bacteriorhodopsin and allow an estimate to be made of the position of the Schiff's base nitrogen. The result limits the assignment of helix G of the sequence to which the chromophore is attached at lysine-216 to helix 2 or 6 of the structure.

The publication costs of this article were defrayed in part by page charge payment. This article must therefore be hereby marked "*advertisement*" in accordance with 18 U.S.C. §1734 solely to indicate this fact.

MATERIALS AND METHODS

Synthesis and Characterization of [$^2H_{11}$]Retinal. The [2,4,4,16,16,16,17,17,17,18,18-$^2H_{11}$]retinal (Fig. 1) was synthesized according to the methods described (8–21). The product was purified by chromatography (5% ether/hexane; silica gel, <230 mesh) and characterized by UV spectroscopy, ^1H NMR and mass spectroscopy. The UV spectrum in ethanol had its maximum at 380 nm and had the same shape and extinction coefficient as that of undeuterated retinal. The ^1H NMR spectrum of the deuterated retinal is shown in Fig. 2. The chemical shifts are in agreement with values in the literature (22) and have the following values. δ: 1.44 (1H,C_2), 1.59 (H_2O), 1.68 (s, 1H, 5-C^2H_2H), 2.05 (s, 3H, 9-CH_3), 2.37 (s, J_{HH}, 3H, 13-CH_3), 5.99 (d, J_{HH} = 8 Hz, 1H, H14), 6.18 (d, J_{HH} = 16 Hz, 1H, H8), 6.21 (d, J_{HH} = 11.5 Hz, 1H, H10), 6.39 (d, J_{HH} = 16 Hz, 1H, H7), 6.40 (d, J_{HH} = 14 Hz, 1H, H12), 7.14 (dd, $J_{H10,H11}$ = 12 Hz, $J_{H11,H12}$ = 14 Hz, 1H, H11), 7.29 ($CHCl_3$), 10.13 (d, J_{HH} = 8 Hz, 1H, H15).

The lack of a signal at δ = 1.03 ppm shows that the methyl groups of carbon 16 and 17 are fully deuterated (10). From the signal at δ = 1.44 ppm, we conclude that the methyl group at carbon-5 contains one proton. Position 4 is furthermore completely deuterated and position 2 only 50% deuterated. These results are to be expected on the basis of the synthetic pathway (8–21). Whether position 3 is deuterated cannot be decided from the ^1H NMR spectrum because of the overlap with the H_2O peak at this δ. The mass spectrum of the deuterated retinal had its main peak at 295, indicating that 11 deuterons were incorporated. On the basis of the ^1H NMR spectrum, the mass spectrum, and the reaction scheme, we conclude that the end product of the synthesis corresponds to the structure represented in Fig. 1.

Regeneration of the Retinal$^-$ Mutant JW5. Retinal or [$^2H_{11}$]retinal was added to the growth medium of mutant strain JW5 and purple membranes were harvested as described (7). The absorption spectra of purple membranes regenerated with retinal and [$^2H_{11}$]retinal are shown in Fig. 3. The ratios of the absorbances at 280 nm and 568 nm are 1.56 and 1.48, respectively, as expected for native purple membrane. The x-ray diffraction pattern of these samples was identical to that of native purple membrane.

Neutron Diffraction Experiments. The experiments were carried out as described (7) except for the following changes. The oriented membrane samples were prepared by drying in 80% relative humidity. Before the beginning of the diffraction experiments, the samples were equilibrated in 100% relative humidity for at least 24 hr. During the diffraction experiments, the samples were enclosed in a cylindrical aluminum can (wall thickness, 0.4 mm) at a relative humidity of 100%.

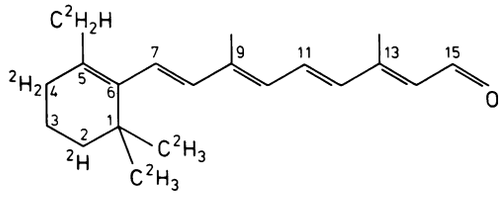

FIG. 1. Chemical structure of the synthetic [$^2H_{11}$]retinal as determined by ^1H NMR and mass spectroscopy.

The retinal and [$^2H_{11}$]retinal samples contained 135 mg and 142 mg of bacteriorhodopsin, respectively. For each sample, two independent data sets were collected to eliminate systematic errors and to test for reproducibility. Each run lasted for the same number of monitor counts, ≈24 hr. The data were collected on the D-16 diffractometer of the High Flux Reactor of the Institut Laue-Langevin (Grenoble). The mosaic spread for both samples had a full width at half height of only 7°, indicating excellent orientation.

RESULTS

Fig. 4 shows the raw intensity data from the position sensitive detector (*a*, undeuterated; *b*, deuterated). The observed intensities were indexed on a hexagonal lattice with unit cell dimension of 63 Å. The (*h,k*) reflection indices are indicated above the corresponding diffraction peaks. The quality of the data is considerably better than in our previous experiments (7). This can be seen most easily by comparing the (*5,2*) and (*6,2*) reflections between the two experiments. Whereas these reflections were at best discernible as shoulders in our previous work (7), they are much better resolved in the present data. The very small mosaic spread of only 7° (full-width at half-height) is probably responsible for this improvement. The intensity differences between Fig. 4 *a* and *b* are expected to be small. Clear changes can nevertheless be observed in the (*1,0*), (*2,0*), and (*4,0*) reflections. The background due to the incoherent scattering of the samples was subtracted and the integrated intensities were corrected by a Lorentz factor of $(h^2 + hk + k^2)^{1/2}$, which is appropriate for a well-oriented sample with a mosaic spread of only 7° (full width) (23). The mosaic spread was identical in the undeuterated and deuterated samples, so that both data sets were corrected by the same Lorentz factor. The absorption and projection corrections were shown to be negligible (5). Since the change in total scattering power of the unit cell due to the deuteration of the cyclohexene ring is very small, the structure factors were scaled in such a way that the sum of the intensities of the undeuterated and deuterated samples became equal (24). Before scaling, the two sums differed by <1%. The values of the differences in the structure factors for the deuterated and undeuterated samples ($\Delta F = |F_D| - |F_H|$) are collected in the second and third columns of Table 1. ΔF_a and ΔF_b refer to the two independently collected data sets. Comparison of the two columns shows good agreement—in particular, all of the signs are the same. By using ΔF_a or ΔF_b as Fourier coefficients, Fourier difference maps were generated using the phase information from the electron diffraction work [last column of Table 1 (25)]. For nonequivalent reflections, which overlap in the powder pattern, the intensity $I(r)$ was split into the squared structure factors F^2 (h,k) with $h^2 + hk + k^2 = r$ according to their ratios in the electron diffraction pattern (25). This approximation as well as the use of the electron microscope phase information have recently been discussed in detail (26). Model calculations showed that at the present resolution these approximations, in the framework of the Fourier difference approach, lead to the correct result for the position of the label, provided that the difference in scattering length between undeuterated and deuterated label is small (26). This condition is satisfied in the present case. The results of the Fourier difference synthesis using ΔF_a and ΔF_b, including all reflections up to and including (*5,2*), are shown in Fig. 5 *a* and *b*, respectively. The last well-resolved reflection in Fig. 4 is (*7,1*). Since no differences in intensity beyond (*5,2*) were observed, however, both native and Fourier difference maps were calculated by summing the contributions up to and including (*5,2*) corresponding to a resolution of 8.7 Å. As expected on the basis of the agreement between the Fourier coefficients ΔF_a and ΔF_b, the two Fourier difference maps of Fig. 5 *a* and *b* are very similar. For clarity, only the six positive contour lines are shown, ranging in steps of 16.7% from 0 (not shown) to 100% of the positive difference density. Both maps have one major maximum at the same position, which is 50% higher than the next highest feature.

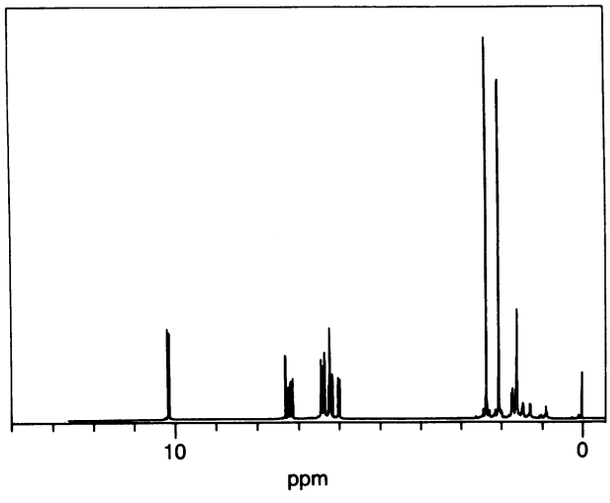

FIG. 2. The ^1H NMR spectrum (270 MHz) of [$^2H_{11}$]retinal in C^2HCl_3 (tetramethylsilane as reference).

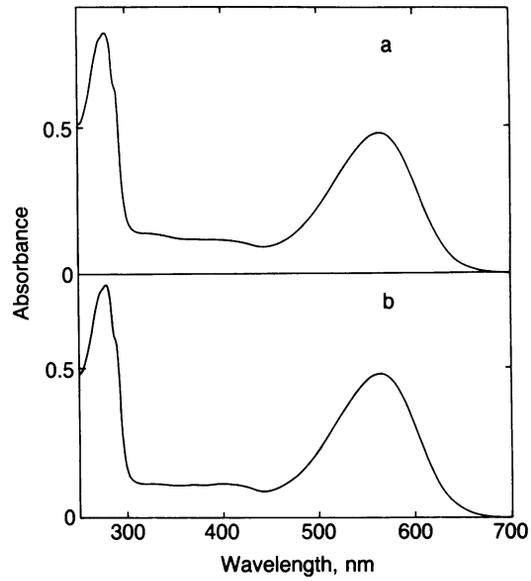

FIG. 3. Absorption spectra of suspensions of light-adapted purple membranes regenerated with retinal (*a*) and with [$^2H_{11}$]retinal (*b*). The spectra were taken with a Shimadzu 240-UV spectrophotometer with integrating sphere.

To investigate the possible significance of the secondary maxima, refinement and model calculations were carried out. In the refinement procedure, the position and occupancy of the label site corresponding to the major maximum are varied until a minimum is found in the "lack of closure" summed

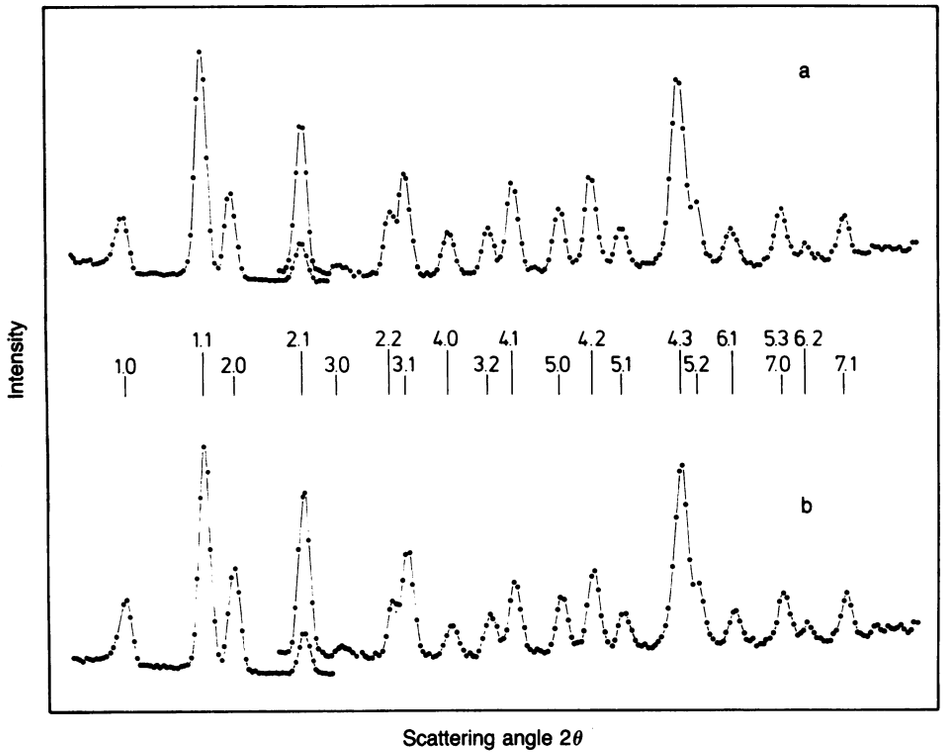

FIG. 4. Neutron diffraction intensities of oriented purple membranes from regenerated JW5 mutants as a function of the detector angle 2θ. Starting with the (2,1) reflection, the vertical scale has been expanded by a factor of 3.95. (*a*) Reconstituted with retinal. (*b*) Reconstituted with [$^2H_{11}$]retinal. The outputs of the position-sensitive detector are shown before the application of corrections. Both samples were in the beam for the same number of monitor counts. The reflections are indexed on the basis of a hexagonal lattice with unit cell dimension of 63 Å. From left to right, 2θ for the data points ranges from 2.25° to 40.05°.

over all reflections (27). This procedure, which gets around some of the limitations of the Fourier difference approach, has been discussed and described in more detail elsewhere (27–29). The label is assumed to be a point. Using as input the coordinates of the main maximum in the Fourier difference map of Fig. 5*a* ($x = -0.19$, $y = 0.14$), the refinement calculation returns final label coordinates of $x = -0.19$ and $y = 0.14$ with differences only in the third decimal. Using the "refined" F_D values, new Fourier difference coefficients ΔF_{ref} were calculated. These are collected for the "a" data set in the fourth column of Table 1. The corresponding Fourier difference map is shown in Fig. 6. The main maximum, which has not changed position, is now twice as high as the highest secondary maximum. Interestingly enough, the secondary maxima remain close to their original positions although no density was placed in these regions. Comparing ΔF_{ref} with ΔF_a, we observe that refinement leads to a change

Table 1. Structure factor differences

(*h*, *k*)	ΔF_a	ΔF_b	ΔF_{ref}	ΔF_{mod}	Phase, degrees
(*1*, *0*)	11.5	9.8	3.6	3.8	342
(*1*, *1*)	−2.2	−1.1	3.7	4.0	162
(*2*, *0*)	22.1	21.9	8.9	9.7	190
(*2*, *1*)	3.2	3.6	2.9	3.3	210
(*1*, *2*)	6.6	7.5	0.5	1.4	312
(*3*, *0*)	3.7	3.1	−0.1	0.4	96
(*2*, *2*)	−8.4	−4.9	−5.4	−5.6	118
(*3*, *1*)	2.2	2.3	0.6	1.6	188
(*1*, *3*)	0.5	0.6	−4.5	−4.7	120
(*4*, *0*)	−16.1	−9.5	−11.9	−12.2	282
(*3*, *2*)	−3.5	−1.4	0.3	−0.9	5
(*2*, *3*)	−2.3	−0.9	3.9	3.7	342
(*4*, *1*)	−15.2	−11.5	−6.8	−7.1	318
(*1*, *4*)	−11.7	−8.9	−5.2	−6.8	308
(*5*, *0*)	−7.3	−7.3	−0.3	0.3	345
(*4*, *2*)	−2.0	−2.6	−7.9	−7.8	103
(*2*, *4*)	−6.1	−7.7	−5.3	−5.1	240
(*5*, *1*)	−0.6	−2.1	6.4	8.4	28
(*1*, *5*)	−2.1	−7.6	−7.8	−8.4	268
(*4*, *3*)	−3.7	−1.0	−3.2	−2.2	125
(*3*, *4*)	−2.3	−0.6	−3.4	−5.1	162
(*5*, *2*)	2.0	2.2	1.7	2.3	130
(*2*, *5*)	0.9	0.9	−3.3	−2.7	272

$\Delta F = |F_D| - |F_H|$. ΔF_a and ΔF_b are the experimental structure factor differences for the two independently collected data sets. ΔF_{ref} and ΔF_{mod} are the calculated structure factor differences from the refinement and model calculations, respectively.

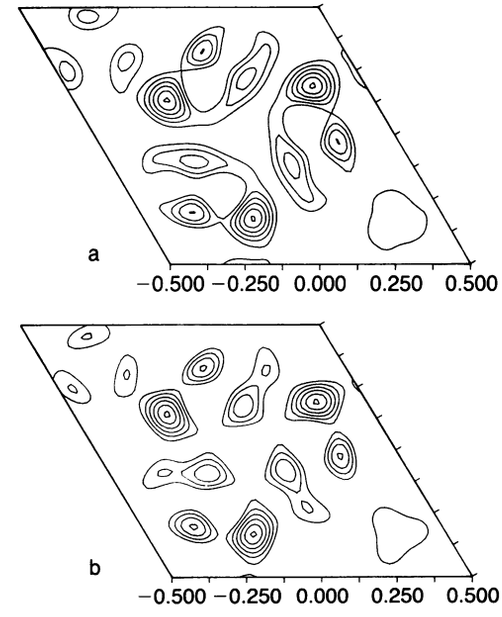

FIG. 5. Fourier difference maps for the center of deuteration of the cyclohexene ring of retinal. Only positive contours are shown, ranging in steps of 16.7%, from 0% (not shown) to 100% of the positive difference density. The side of the hexagonal unit cell corresponds to 63 Å. *a* and *b* are the results for two independent sets of measurements.

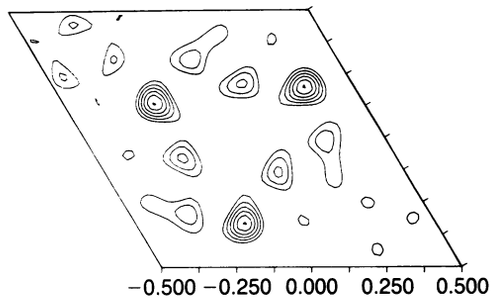

FIG. 6. Fourier difference map after refinement in reciprocal space of the data used in Fig. 5*a*.

in sign of 7 of the 23 ΔF values. In 5 of the 7 cases, either ΔF_{ref} or ΔF_a was close to zero. Refinement of the "b" data set led to the same position for the maximum in the Fourier difference map and to very similar ΔF_{ref} values. To show that the amplitude of the difference density observed in Fig. 5*a* corresponds to that expected for the replacement of 11 protons by 11 deuterons, model calculations were performed as described (26). The map was put on an absolute scale in the following way. The neutron structure factors for the undeuterated sample were transformed into a density map on a grid of points (60 × 60) for the unit cell using the electron microscope phases. The total scattering length of an average helix was determined by integration over the appropriate region in space. The correct scattering density for the label on this scale was determined by multiplying this average helical scattering length by the ratio of the calculated scattering length of the label (11 deuterons minus 11 protons; 114 Fermi) and the calculated average scattering length of one helix (567 Fermi). This extra density was added to the density of the undeuterated sample at the point ($x = -0.19$, $y = 0.14$) determined in the refinement procedure. By transforming this density, a set of predicted structure factors for the deuterated sample was obtained. The predicted Fourier difference coefficients ΔF_{mod} (Table 1, column 5) are in excellent agreement with the coefficients ΔF_{ref} from the refinement procedure. The agreement with the experimentally observed ΔF_a values is likewise good. There are only six changes in sign, occurring for reflections with relatively small difference coefficients. This result shows that the Fourier difference map of Fig. 5*a* has indeed the appropriate amplitude expected for the label. To show this graphically, rather than through the agreement between columns 2 and 5 of Table 1, we reproduce in Fig. 7 the Fourier difference map with the coefficients ΔF_{mod}. The agreement with Figs. 5 and 6 is excellent. Another way to test whether the difference density has about the right amplitude is to compare the maximum in the Fourier difference map for the chain deuterated retinal (10 deuterons) from our previous work (7) with the corresponding maximum for the ring deuterated retinal (11 deuterons), after normalizing the intensities. Use of this relative standard avoids the problem of absolute scaling. The two numbers differ by only 20%. In both the refinement and model calculations, the label density was placed at the single site corresponding to the maximum of Fig. 5*a*. We note from Figs. 6 and 7 that in both cases a difference density is predicted that includes secondary maxima very close to the secondary maxima in the Fourier difference map of Fig. 5*a*. We may therefore conclude that these subsidiary maxima do not correspond to true label density (such as secondary retinal binding sites) but are rather due to cut-off and phase errors as well as intrinsic errors in the Fourier difference method.

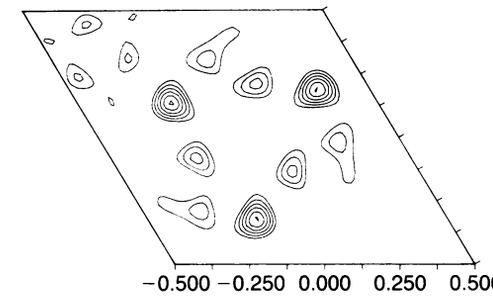

FIG. 7. Fourier difference map predicted on the basis of model calculations in which a difference density corresponding to the strength of the label is placed at the position determined in the refinement calculation.

The 85%, 90%, 95%, and 99% contour lines from Fig. 5*a* are redrawn in Fig. 8 superimposed on the native structure (circular set of contour lines). The native structure was calculated by using the intensities of Fig. 5*a* and the phases from electron diffraction. It is clear from Fig. 8 that the center of deuteration of the cyclohexene ring is located between helices 3, 4, 5, and 6, closest to helix 4.

DISCUSSION

Compared with our previous work with chain-deuterated retinal (7), several improvements were made in the diffraction experiment and in the data analysis. The quality of the data, in particular the resolution of the individual diffraction peaks, was much improved by using better oriented samples at 100% relative humidity. Two independent data sets were collected to test the reproducibility of our data and to look for errors due to beam and detector instabilities. Analysis of the two data sets led, within experimental error, to the same Fourier difference map. The position of the label was refined and model calculations were carried out to show that the observed difference density had the right amplitude for a label containing 11 deuterons. It was shown that the secondary maxima are mainly due to phase errors and intrinsic errors of the Fourier difference approach, since they also occurred in the model calculation in which the difference density was only placed at the main maximum.

As in our previous work, the synthetic retinal was characterized by ^{1}H NMR and mass spectroscopy to establish the label distribution shown in Fig. 1. For the undeuterated

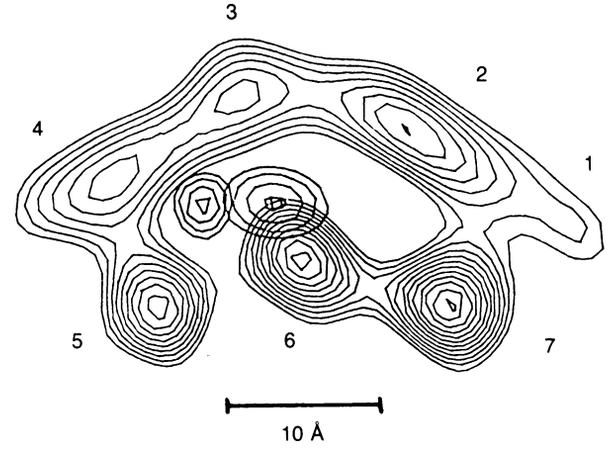

FIG. 8. Summary of the neutron diffraction results for JW5 mutants regenerated with chain-deuterated (7) and ring-deuterated retinal. Superimposed on the structure of bacteriorhodopsin, as determined from the neutron diffraction intensities, are shown the 85%, 90%, 95%, and 99% contour lines for the positive difference density from these experiments. The oval set of lines near helix 6 corresponds to the center of deuteration of the polyene chain (C-11). The circular set of lines to the left corresponds to the center of deuteration of the cyclohexene ring.

reference, we did not use normal purple membranes, but rather prepared regenerated JW5 samples in exactly the same way as the deuterated samples. We consider this to be of crucial importance.

Our recent result on the position of the middle of the polyene chain (7) and our current result concerning the cyclohexene ring are summarized in Fig. 8. The figure shows that the distance between the projected centers of deuteration of the chain (C-11) and of the ring (near the middle of the C-5–C-6 bond, inside the ring) is ≈4.9 Å. The expected distance is estimated to lie between 4.3 and 5.7 Å. This calculation takes into account that the 6-s bond has the planar trans conformation (30) and that the polyene chain makes an angle of ≈20° with the plane of the membrane (6). The uncertainty is mainly due to lack of information about the orientation of the plane containing the chain and the ring with respect to the plane of the membrane. The result of Fig. 8 about the projected distance between the two centers of deuteration is thus fully consistent with our present knowledge about the conformation and orientation of the chromophore. The direction from the cyclohexene ring to the Schiff base is from left to right in Fig. 8. It is tempting to draw a line through the two difference peaks and to extrapolate to the position of the Schiff's base taking into account the 20° orientation of the polyene chain. Such an extrapolation is subject to at least two uncertainties: the lack of geometrical information mentioned above and the effect of the 50% 13-cis retinal in our dark-adapted sample. The result of the extrapolation is that the Schiff's base nitrogen is located halfway between the axes of helices 2 and 6. The maximal distance of the lysine nitrogen from the helical axis, assuming the lysine is extended perpendicular to the axis, is ≈8 Å. Only the axes of helices 2 and 6 fall within a circle of radius 8 Å drawn around this point. Since retinal is attached to lysine-216 of helix G in the sequence, it follows that G is either 2 or 6. Since the axes of the other helices in Fig. 8 (*3,1,7*) fall clearly outside the circle, it is unlikely that this conclusion will be altered. Three previous structural studies provide information on the location of helix G (23, 28, 31). Our result is in disagreement with the conclusion of one of these reports, in which G is assigned to helix 4 (31). It is apparent from Fig. 8 that there is no way to resolve this discrepancy.

We have used selectively deuterated retinals to obtain detailed and localized information on the position and orientation of parts of the chromophore. In previous neutron diffraction work on the location of retinal, perdeuterated retinal containing 28 deuterons was used (4, 5). Since in a projection onto the plane of the membrane the elongated density corresponding to the chromophore has a length of ≈14 Å, these experiments allowed determination of only the center of deuteration of the whole retinal. With 15 deuterons in the ring and 13 in the chain, the center of deuteration of perdeuterated retinal is near C-8 assuming the C-6–C-7 bond to be trans (30). The two previous experiments came to opposite conclusions concerning the location of the center of deuteration. This discrepancy is discussed in more detail in ref. 7. The results in ref. 5 are near our ring position and consistent with both of our experiments (between the ring and the middle of the chain), whereas the results of ref. 4 are near helix 2. The latter result must be incorrect.

It appears to be worthwhile to complement the present work with a synthetic retinal deuterated in the Schiff's base region and to use the three partially deuterated retinals to determine the distances from the membrane surfaces.

We thank J. Lugtenburg for his advice on the synthesis of [$^2H_{11}$]retinal. We are grateful to H.-J. Plöhn and G. Büldt for the use of their model calculation program; to J. Finer-Moore for help with the refinement calculations; to J. Torbet of the Institut Laue-Langevin for his support as local contact on the D-16 diffractometer; to R. Henderson for providing us with the phases and structure factor ratios from the electron diffraction work. This project was supported by Grant 03 B72C019 of the Bundesministerium für Forschung und Technologie.

1. Stoeckenius, W. & Bogomolni, R. A. (1982) *Annu. Rev. Biochem.* **52,** 587–616.
2. Kouyama, T., Kimura, Y., Kinosita, K. & Ikegami, A. (1982) *J. Mol. Biol.* **153,** 337–359.
3. Rehorek, M., Dencher, N. A. & Heyn, M. P. (1983) *Biophys. J.* **43,** 39–45.
4. King, G. I., Mowery, P. C., Stoeckenius, W., Crespi, H. L. & Schoenborn, B. P. (1980) *Proc. Natl. Acad. Sci. USA* **77,** 4726–4730.
5. Jubb, J. S., Worcester, D. L., Crespi, H. L. & Zaccai, G. (1984) *EMBO J.* **3,** 1455–1461.
6. Heyn, M. P., Cherry, R. J. & Mueller, U. (1977) *J. Mol. Biol.* **117,** 607–620.
7. Seiff, F., Wallat, I., Ermann, P. & Heyn, M. P. (1985) *Proc. Natl. Acad. Sci. USA* **82,** 3227–3231.
8. Lugtenburg, J. (1985) *Pure Appl. Chem.* **57(5),** 753–762.
9. Fransen, M. R., Palings, I., Lugtenburg, J., Jansen, P. A. A. & Groenendijk, G. W. T. (1980) *Recl. Trav. Chim. Pays-Bas* **99,** 384–391.
10. Pardoen, J. A., Neijenesch, H. N., Mulder, P. P. J. & Lugtenburg, J. (1983) *Recl. Trav. Chim. Pays-Bas* **102,** 341–347.
11. Pardoen, J. A., Winkel, C., Mulder, P. P. J. & Lugtenburg, J. (1984) *Recl. Trav. Chim. Pays-Bas* **103,** 135–141.
12. Lugtenburg, J. (1984) in *Spectroscopy of Biological Molecules*, eds. Sandorfy, C. & Theophanides, T. (Reidel, Dordrecht, The Netherlands), pp. 447–455.
13. Ramsden, H. E., Leebrick, J. R., Rosenberg, S. D., Miller, E. H., Walburn, J. J., Balint, A. E. & Cserr, R. (1957) *J. Org. Chem.* **22,** 1602–1605.
14. Saucy, G. & Marbet, R. (1967) *Helv. Chim. Acta* **50,** 1158–1167.
15. Saucy, G. & Marbet, R. (1967) *Helv. Chim. Acta* **50,** 2091–2100.
16. Albavella, J. P. (1977) *J. Org. Chem.* **42,** 2009.
17. Corey, L. J., Enders, D. & Bock, M. G. (1976) *Tetrahedron Lett.* **17,** 7–10.
18. Attenburrow, J., Cameron, A. F. B., Chapman, J. H., Evans, R. M., Hems, B. A., Jensen, A. B. A. & Walker, T. (1952) *J. Chem. Soc.*, 1094–1111.
19. Courtin, J. M. L., 't Lam, G. K., Peters, A. J. M. & Lugtenburg, J. (1985) *Recl. Trav. Chim. Pays-Bas* **104,** 281–288.
20. Dugger, R. W. & Heathcock, C. H. (1980) *Synth. Commun.* **10(7),** 509–515.
21. Thomas, A. F. (1971) *Deuterium Labelling in Organic Chemistry* (Meredith, New York), pp. 122–123.
22. Patel, D. (1969) *Nature (London)* **221,** 825.
23. Wallace, B. A. & Henderson, R. (1982) *Biophys. J.* **39,** 233–239.
24. Blundell, T. L. & Johnson, L. N. (1976) *Protein Crystallography* (Academic, New York).
25. Unwin, P. N. T. & Henderson, R. (1975) *J. Mol. Biol.* **94,** 425–440.
26. Plöhn, H.-J. & Büldt, G. (1986) *J. Appl. Cryst.* **19,** 255–261.
27. Dickerson, R. E., Weinzierl, J. E. & Palmer, R. A. (1968) *Acta Cryst.* **B24,** 997–1003.
28. Katre, N. V., Finer-Moore, J., Stroud, R. M. & Hayward, S. B. (1984) *Biophys. J.* **46,** 195–204.
29. Seiff, F., Wallat, I., Westerhausen, J. & Heyn, M. P. (1986) *Biophys. J.*, in press.
30. Harbison, G. S., Smith, S. O., Pardoen, J. A., Courtin, J. M. L., Lugtenburg, J., Herzfeld, J., Mathies, R. A. & Griffin, R. G. (1985) *Biochemistry* **24,** 6955–6962.
31. Trewhella, J., Anderson, S., Fox, R., Gogol, E., Khan, S., Zaccai, G. & Engelman, D. M. (1983) *Biophys. J.* **42,** 233–241.